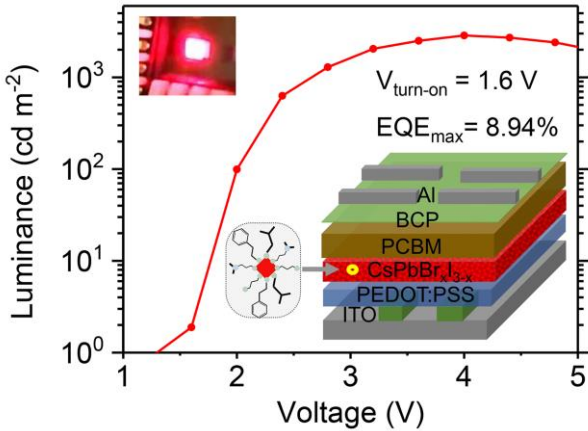


# CsPbBr<sub>x</sub>I<sub>3-x</sub> thin films with multiple ammonium ligands for low turn-on pure-red perovskite light-emitting diodes

Maowei Jiang, Zhanhao Hu, Luis K. Ono, and Yabing Qi (✉)

Energy Materials and Surface Sciences Unit (EMSSU), Okinawa Institute of Science and Technology Graduate University (OIST), 1919-1 Tancha, Onna-son, Okinawa 904-0495, Japan

## TABLE OF CONTENTS (TOC)

<p><b>CsPbBr<sub>x</sub>I<sub>3-x</sub> thin films with multiple ammonium ligands for low turn-on pure-red perovskite light-emitting diodes</b></p> <p>Maowei Jiang, Zhanhao Hu, Luis K. Ono, and Yabing Qi*</p> <p>Okinawa Institute of Science and Technology Graduate University (OIST), Japan</p>	 <p>CsPbBr<sub>x</sub>I<sub>3-x</sub> thin films featuring nano-sized crystallites were prepared via incorporating multiple ammonium ligands in a one-step spin-coating route. The CsPbBr<sub>x</sub>I<sub>3-x</sub> LED, adopting a conventional device structure of ITO/PEDOT:PSS/CsPbBr<sub>x</sub>I<sub>3-x</sub>/PCBM/BCP/Al, showed a pure-red color at 659 nm, low turn-on voltage (1.6 V), high brightness (2859 cd m<sup>-2</sup>) and high external quantum efficiency (8.94%).</p>
---	--

Yabing Qi, <https://groups.oist.jp/emssu/yabing-qi>

# CsPbBr<sub>x</sub>I<sub>3-x</sub> thin films with multiple ammonium ligands for low turn-on pure-red perovskite light-emitting diodes

Maowei Jiang, Zhanhao Hu, Luis K. Ono, and Yabing Qi (✉)

Energy Materials and Surface Sciences Unit (EMSSU), Okinawa Institute of Science and Technology Graduate University (OIST), 1919-1 Tancha, Onna-son, Okinawa 904-0495, Japan

© Tsinghua University Press and Springer-Verlag GmbH Germany, part of Springer Nature 2020

**Received:** day month year / **Revised:** day month year / **Accepted:** day month year (automatically inserted by the publisher)

## ABSTRACT

All-inorganic  $\alpha$ -CsPbBr<sub>x</sub>I<sub>3-x</sub> perovskites featuring nano-sized crystallites show great potential for pure-red light-emitting diode (LED) applications. Currently, the CsPbBr<sub>x</sub>I<sub>3-x</sub> LEDs based on nano-sized  $\alpha$ -CsPbBr<sub>x</sub>I<sub>3-x</sub> crystallites have been fabricated mainly via the classical colloidal route including a tedious procedure of nanocrystal synthesis, purification, ligand or anion exchange, film casting, etc. With the usually adopted conventional LED device structure, only high turn-on voltages (> 2.7) have been achieved for CsPbBr<sub>x</sub>I<sub>3-x</sub> LEDs. Moreover, this mix-halide system may suffer from severe spectra-shift under bias. In this report, CsPbBr<sub>x</sub>I<sub>3-x</sub> thin films featuring nano-sized crystallites are prepared by incorporating multiple ammonium ligands in a one-step spin-coating route. The multiple ammonium ligands constrain the growth of CsPbBr<sub>x</sub>I<sub>3-x</sub> nanograins. Such CsPbBr<sub>x</sub>I<sub>3-x</sub> thin films benefit from quantum confinement. The corresponding CsPbBr<sub>x</sub>I<sub>3-x</sub> LEDs, adopting a conventional LED structure of indium-doped tin oxide (ITO)/poly(3,4-ethylenedioxythiophene):poly(styrenesulfonate) (PEDOT:PSS)/CsPbBr<sub>x</sub>I<sub>3-x</sub>/[6,6]-phenyl C61 butyric acid methyl ester (PCBM)/bathocuproine (BCP)/Al, emit pure-red color at Commission Internationale de l'éclairage (CIE) coordinates of (0.709, 0.290), (0.711, 0.289), etc., which represent the highest color-purity for reported pure-red perovskite LEDs and meet the Rec. 2020 requirement at CIE (0.708, 0.292) very well. The CsPbBr<sub>x</sub>I<sub>3-x</sub> LED shows a low turn-on voltage of 1.6 V, maximum external quantum efficiency of 8.94%, high luminance of 2859 cd m<sup>-2</sup> and good color stability under bias.

## KEYWORDS

CsPbBr<sub>x</sub>I<sub>3-x</sub> thin film; nano-sized crystallites; surface termination; pure-red color; perovskite light-emitting diode; low turn-on voltage

## 1 Introduction

Over the past few years, great efforts have been made for light-emitting applications of lead halide perovskites [1-5], of which one important subject is the pure-red perovskite light-emitting diodes (PeLEDs) with emissions from 630 nm to 660 nm [5-7]. For APbI<sub>3</sub> perovskites, organic A-site cation (such as methylammonium and formamidinium) based perovskites exhibit near-infrared emissions, while all-inorganic  $\alpha$ -CsPbI<sub>3</sub> perovskite intrinsically emits a deep-red color at about 700 nm [4, 8, 9]. From the viewpoint of bandgap, the all-inorganic  $\alpha$ -CsPbI<sub>3</sub> perovskite shows potential in red LEDs. However, CsPbI<sub>3</sub> suffers from phase instability issue, i.e., it readily transforms from metastable black phase to yellow phase at room temperature [8, 10]. To overcome this issue, several methods have been reported, e.g., synthesis of CsPbI<sub>3</sub> nanocrystals (NCs) or quantum dots (QDs) [11], incorporation of bromide ion into CsPbI<sub>3</sub> [12, 13], etc.

Currently, one of the most prevailing ways of devising pure-red all-inorganic PeLEDs is based on colloidal CsPbBr<sub>x</sub>I<sub>3-x</sub> NCs, which have the benefits of (i) the versatile surface chemistry with efficient ligand passivation, (ii) the spatial confinement for exciton recombination, (iii) the phase

stabilization induced by the nano-size effect, and (iv) the color tunability due to Br-incorporation, etc. [5, 6, 11, 14] The CsPbBr<sub>x</sub>I<sub>3-x</sub> NCs are normally synthesized via colloidal route such as hot-injection method, then post-treated by purification, ligand- or anion- exchange, and finally spin-coated onto substrates for further LED fabrication [5, 6, 15]. Note that, the tedious post-treatment procedures may lead to changes of size/morphology and optical properties of perovskite NCs, because ionic perovskite NCs are sensitive to dielectric-constant solvents, which result in the desorption of surface ligands [11, 16-18]. Thereby, seeking alternative options for fabricating CsPbBr<sub>x</sub>I<sub>3-x</sub> NC based thin films beyond the colloidal route is motivated.

On the other hand, the CsPbI<sub>3</sub> QD based LEDs through colloidal route normally exhibit EL above 688 nm, and via inorganic cation substitution such as zinc or strontium in CsPbI<sub>3</sub> QDs can further blue-shift their EL to 678 nm [19-24], which is not good enough to meet the requirement of Rec. 2020 color gamut at CIE (0.708, 0.292) [25]. Efforts to realize pure-red EL emitting (e.g., 630 nm ~ 660 nm) should be made. Indeed, in our literature survey list in Table S1 (see Electronic Supplementary Material (ESM)), most reports of efficient all-inorganic PeLEDs in the pure-red region are based on the mix-halide system, of which the color tunability benefits from

bandgap broadening induced by excess Br-incorporation [5, 6, 22, 26]. But unfortunately in these studies, most cases fail in sustaining their color purity because of halide ion mobility and phase segregation under bias [5, 6, 27–29]. For example, Kido et al. reported a mix-halide  $\text{CsPbBr}_x\text{I}_{3-x}$  QD based LED adopting a conventional LED device structure (Table S1), which showed an external quantum efficiency (EQE) of 21.3%, turn-on voltage of 2.8 V, luminance of  $500 \text{ cd m}^{-2}$  at 653 nm (Table S1); but the EL spectra showed red-shift under bias [5]. Besides, for pure-red  $\text{CsPbBr}_x\text{I}_{3-x}$  LEDs, low turn-on voltage, high luminance, high EQE and good color stability still cannot be simultaneously achieved yet. Up to date, with an inverted LED device structure, the reported highest EQE of  $\text{CsPbBr}_x\text{I}_{3-x}$  LEDs in pure-red wavelength range (e.g., 630 ~ 660 nm) did not exceed 6.3% (Table S1) [6, 23]. For those adopting a conventional LED device structure, the lowest turn-on voltage was about 2.7 V (Table S1) [5, 30], which is much higher than their emission photon energy about 1.9 V; and the record luminance was about  $2671 \text{ cd m}^{-2}$  with a peak EQE of 3.55% reported by Yao and co-workers [6].

Exploring new strategies to improve the performance of all-inorganic pure-red  $\text{CsPbBr}_x\text{I}_{3-x}$  LEDs, simultaneously with low turn-on voltage, high luminance, high EQE and good color stability, is still an open challenge. In this report, a new route to fabrication of  $\text{CsPbBr}_x\text{I}_{3-x}$  thin films, featuring nano-sized crystallites, is developed via a simple one-step spin-coating

method, which simplifies the fabrication procedure in comparison with the classical colloidal route. The  $\text{CsPbBr}_x\text{I}_{3-x}$  nanograins in the thin films are enabled by the surface termination effect of multiple bulky ammonium ligands [31–33]. In addition, the  $\text{CsPbBr}_x\text{I}_{3-x}$  thin films benefit from bandgap broadening by quantum confinement. The  $\text{CsPbBr}_x\text{I}_{3-x}$  thin film based LED with a conventional LED device structure (indium-doped tin oxide (ITO)/poly(3,4-ethylenedioxythiophene):poly(styrenesulfonate) (PEDOT:PSS)/ $\text{CsPbBr}_x\text{I}_{3-x}$ /[6,6]-phenyl C61 butyric acid methyl ester (PCBM)/bathocuproine (BCP)/Al) shows a pure-red color at CIE (0.711, 0.289), low turn-on voltage of 1.6 V, maximum EQE of 8.94%, and high luminance of  $2859 \text{ cd m}^{-2}$ . In addition, the spectra-shift phenomenon under bias has been greatly inhibited, which leads to good color purity.

## 2 Results and discussion

The  $\text{CsPbBr}_x\text{I}_{3-x}$  thin films were fabricated via the typical one-step spin-coating method (Fig. 1(a)). Briefly, the perovskite solution incorporating with multiple ammonium ligands was firstly prepared by dissolving 1 mmol of  $\text{PbI}_2$ , 1 mmol of  $\text{CsI}$ , 0.25 mmol (25% relative to perovskite precursor) of phenethylammonium iodide (PEAI), 0.25 mmol (25%) of isobutylammonium bromide (IBAB), 0.1 mmol (10%) of 1,3-propanediammonium bromide (PDAB) and 0.1 mmol (10%) of N,N-dimethyl-1,3-propanediammonium bromide (DMPDAB)

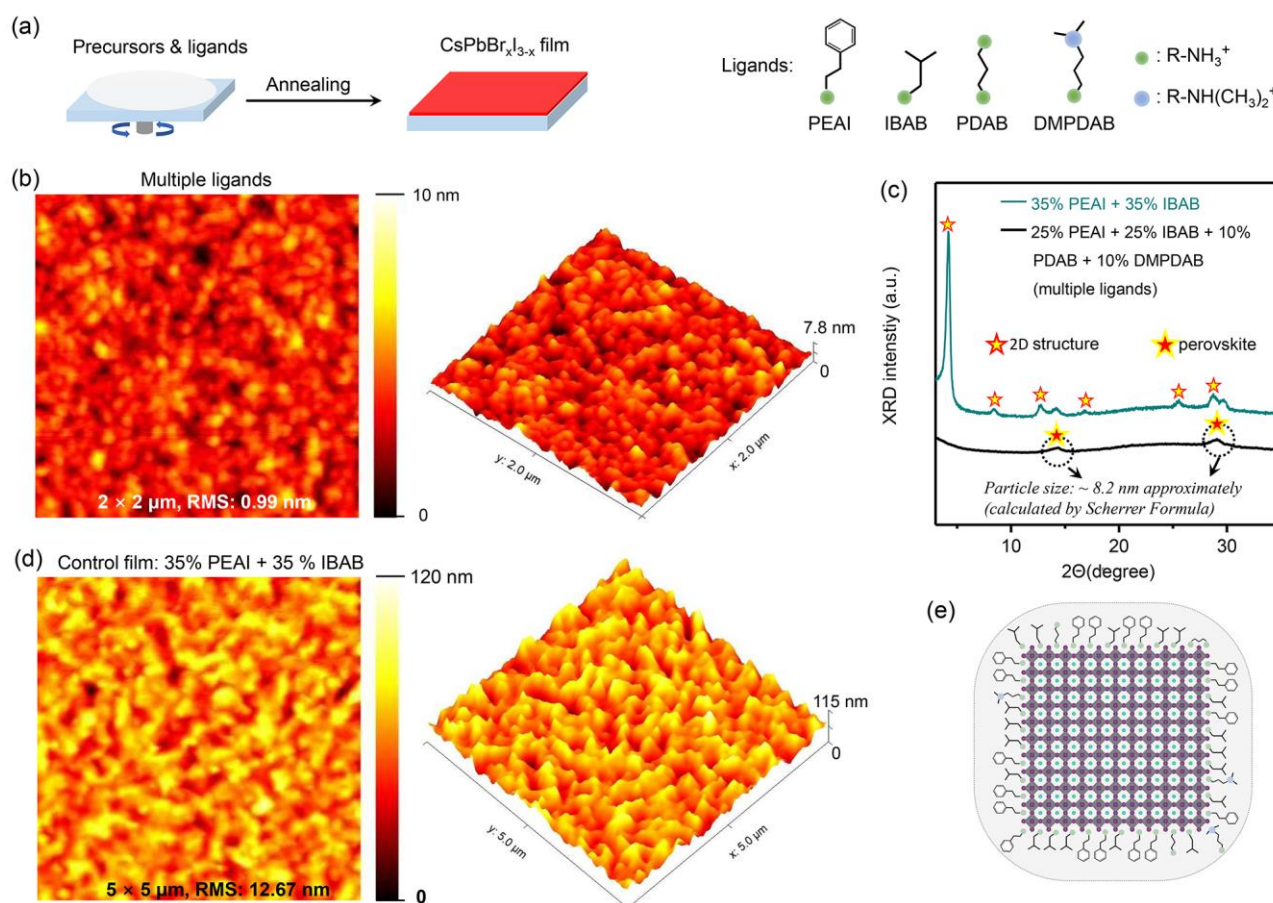


**Figure 1** (a) Illustration of one-step spin-coating method to prepare  $\text{CsPbBr}_x\text{I}_{3-x}$  films. The chemical structures of multiple ammonium ligands are shown in the right panel. (b) Tapping-mode AFM images of the  $\text{CsPbBr}_x\text{I}_{3-x}$  thin film incorporating with multiple (four) ligands. The film RMS roughness is about 0.99 nm; the scan area is  $2 \times 2 \mu\text{m}$ . (c) XRD curves of  $\text{CsPbBr}_x\text{I}_{3-x}$  film incorporating with multiple ligands and control film incorporating with 35% PEAi and 35% IBAB. (d) AFM images of the control film incorporating with 35% PEAi and 35% IBAB. The film RMS roughness is about 12.67 nm; the scan area is  $5 \times 5 \mu\text{m}$ . (e) A schematic drawing showing a nano-sized grain with multiple ammonium ligands on its surface.

in 3.33 ml of dimethyl sulfoxide (DMSO). The concentration of perovskite precursor was indicated as 0.3 M. The as-prepared precursor solution was spin-coated onto PEDOT:PSS substrate (see more details in Experimental section), which was then annealed for better crystallization. The typical annealing temperature was 100°C if not stated otherwise. We suggest that the Br content in  $\text{CsPbBr}_x\text{I}_{3-x}$  may be reduced to a small amount so as to inhibit the robust spectra-shift under bias. Herein, a small ratio of Br anion, 16.7% approximately, was introduced from the ammonium bromide ligands, taking into account the total ratio of Br/(Br + I) in the perovskite precursors and ligands.

The surface morphology information of the  $\text{CsPbBr}_x\text{I}_{3-x}$  thin film incorporating with multiple ammonium ligands was studied by atomic force microscope (AFM). The AFM images in Fig. 1(b) and S1 reveal no large grains existing in the film and uniform perovskite grains within nano-sized range are formed. Further calculation of root mean square (RMS) value based on the AFM image in Fig. 1(b) reveals a rather smooth surface of the  $\text{CsPbBr}_x\text{I}_{3-x}$  film, with a very small RMS value of 0.99 nm. This RMS value of the  $\text{CsPbBr}_x\text{I}_{3-x}$  film is even smaller than that ( $\sim 2.43$  nm) of colloidal  $\text{CsPbBr}_x\text{I}_{3-x}$  QD based thin film [6, 21]. Moreover, the scanning electron microscope (SEM) characterization in Fig. S2 further demonstrates the conclusion that uniform perovskite nano-sized grains ( $\sim 8$  nm approximately) are formed in the film incorporating with multiple ammonium ligands. In addition, we performed X-ray diffraction (XRD) measurement to study the crystallinity of the  $\text{CsPbBr}_x\text{I}_{3-x}$  thin films. In Fig. 1(c) and S3, the  $\alpha$ -phase  $\text{CsPbBr}_x\text{I}_{3-x}$  thin film featuring nano-sized crystallites is revealed by the broadened XRD peaks with reduced diffraction intensity [34]. By contrast, the broadened XRD peaks of the  $\text{CsPbBr}_x\text{I}_{3-x}$  thin film in current system are consistent with those of colloidal  $\text{CsPbBr}_x\text{I}_{3-x}$  QDs in previous reports [6, 22]. On the other hand, as a further auxiliary evaluation for the  $\text{CsPbBr}_x\text{I}_{3-x}$  nano-sized crystallites in the film, a calculation based on the Scherrer formula according to the full-width at half maximum (FWHM) of the XRD peaks was performed and the result reveals an approximate size of 8.2 nm for the nanograins. The AFM, SEM and XRD results synergistically demonstrate the formation of  $\text{CsPbBr}_x\text{I}_{3-x}$  thin films featuring nano-sized crystallites, which is consistent with previous reports about perovskite thin films featuring nano-sized crystallites by Rand, Xiao and coworkers [33, 34]. Notably, no obvious layer-stacked structures are observed by the XRD result, which is consistent with the UV-vis absorption spectrum as shown in Fig. S4 [26, 31, 33-36].

For bulky organoammonium ligands, the ammonium groups can only coordinate on the surface of  $\text{CsPbBr}_x\text{I}_{3-x}$  crystallites. In other words, incorporation of bulky organoammonium ligands constrains the growth of perovskite crystallites [32, 34, 37]. To explore this constraining effect, or called as surface termination effect, we initially considered single kind of bulky organoammoniums such as phenethylammonium, butylammonium, n-propylammonium, 1-naphthylmethylammonium, etc., which have been widely studied in perovskite systems; however, single type of these ligands as the surface termination agent tend to stack to form quasi-2D perovskites when the ligand usage was over 40% of perovskite precursor approximately [26, 32, 34, 36, 38-40]. For

example, Huang et al. [26] reported quasi-2D  $\text{CsPbI}_3$  perovskites with 1-naphthylmethylammonium as ligands exhibiting a peak EQE value of 7.3% and maximum luminance of 732  $\text{cd m}^{-2}$  at 694 nm; however, as EL wavelength of the LEDs shifted to 684 nm, the luminance was decreased greatly to 4  $\text{cd m}^{-2}$  with an EQE of 1.2% (Table S1). Choy et al. [38] separately incorporated n-propylammonium, n-butylammonium, n-hexylammonium etc., to prepare quasi-2D  $\text{CsPbI}_3$  perovskites and the corresponding PeLEDs showed a maximum EQE value of 1.84% and luminance of 106  $\text{cd m}^{-2}$  at 658 nm.

In another report, Sargent and coworkers reported a ligand system including two different kinds of ammoniums, phenethylammonium and iso-propylammonium, which reduces the van der Waals interactions of ligands to enhance the phase monodispersity of quasi-2D perovskites [31]. Inspired by this work, a control experiment using two kinds of ammonium ligands including 35% PEA and 35% IBAB was performed. 2D layered structures are formed in this control film, as demonstrated by the XRD curve in Fig. 1(c). The AFM images in Fig. 1(d) and SEM image in Fig. S2(b) reveal a relatively rough surface of this control film with a RMS value of 12.67 nm, and larger perovskite grains are formed. Besides, the PL lifetime measurement result in Fig. S5 shows that the perovskite thin film incorporating with multiple ligands has a longer average PL lifetime of 5.9 ns, and the control film has an average PL lifetime of 2.9 ns. The multiple ammonium ligands demonstrate a better passivation effect for perovskite thin films [32, 33]. Further EL studies based on this control film system show broadening and shifting of EL peaks under increasing voltages (Fig. S6), and the corresponding PeLED shows a maximum EQE value of 1.05% and luminance of 595  $\text{cd m}^{-2}$  at 675 nm (Fig. S6). The optoelectronic performance is not as good as that using our suggested multiple ammonium ligand recipe, which is discussed below.

The polydisperse phases of quasi-2D  $\text{CsPbBr}_x\text{I}_{3-x}$  thin films with two kinds of PEA and IBAB ammonium ligands in above control experiment may be further focused by inhibiting the formation of multi-layered 2D perovskite structures. The question is how to inhibit the periodic stacks of the organic end groups in the ammonium ligands. We propose that it may be realized via random arrangement of multiple ammonium ligands including both the hydrophobic and hydrophilic end groups [32], which can increase the diversity of surface termination agent and reduce the van der Waals interactions of ligands [31, 32, 41]. Based on this proposal, we designed a multiple ammonium ligand recipe, with a small amount of hydrophilic bi-ammonium [32], namely PDAB (10%) and DMPDAB (10%) ligands, replacing a portion of PEA (25% left) and IBAB (25% left) ligands. The PDAB and DMPDAB ligands have been demonstrated to show good passivation effect on perovskites in our previous report [32]. In that report, we explored the effect of the mentioned hydrophilic bi-ammonium (PDAB and DMPDAB) dominated ligand system on the performance of perovskite thin films. In this report, the widely used bulky ammonium ligands with hydrophobic end groups (PEA<sup>+</sup>, IBA<sup>+</sup>, etc) dominated the ligand system, and we intended to use a small portion of hydrophilic bi-ammonium to break the stack trend of these widely used bulky ammonium ligands featuring hydrophobic end groups. As a result, using the multiple ammonium recipe as mentioned above, the  $\text{CsPbBr}_x\text{I}_{3-x}$



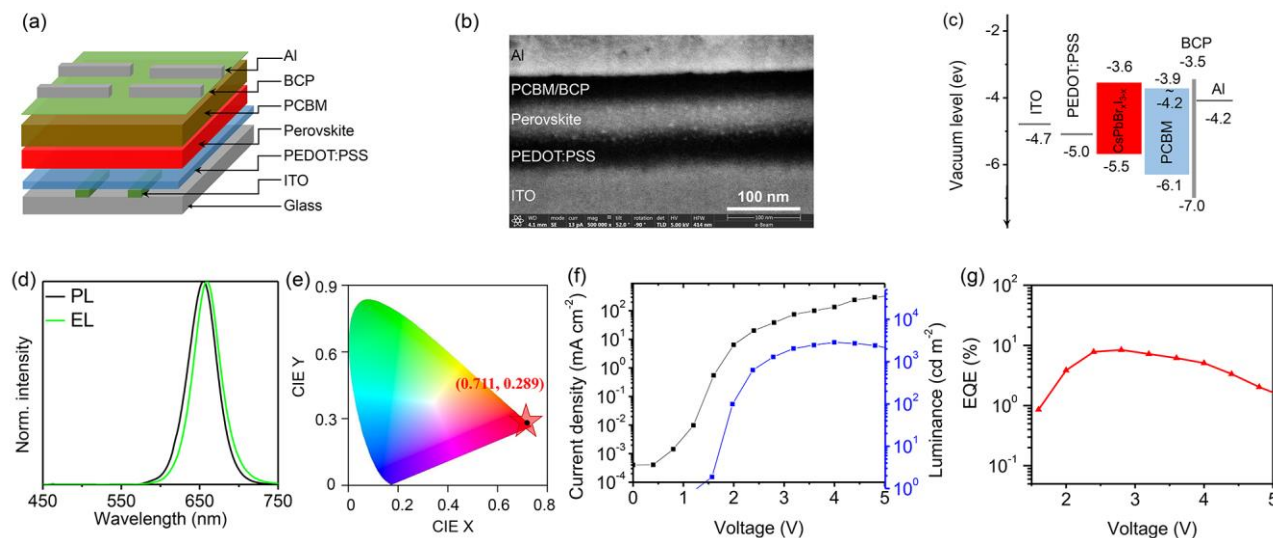


**Figure 2** (a) LED device structure adopted in this work, and its Cross-section SEM image (b) and corresponding energy diagram (c). In (b), the tilt angle (Y direction) is  $52^\circ$ . (d) Normalized (Norm.) PL and EL spectra of the  $\text{CsPbBr}_{x}\text{I}_{3-x}$  film. (e) CIE coordinates of the  $\text{CsPbBr}_{x}\text{I}_{3-x}$  LED. (f) Current density and luminance versus voltage curves of the  $\text{CsPbBr}_{x}\text{I}_{3-x}$  LED. (g) EQE versus voltage curve of the  $\text{CsPbBr}_{x}\text{I}_{3-x}$  LED. The  $\text{CsPbBr}_{x}\text{I}_{3-x}$  thin film was annealed at  $100^\circ\text{C}$ .

thin films featuring nano-sized crystallites are formed and the 2D structures are effectively inhibited. A schematic drawing showing a nano-sized grain in our  $\text{CsPbBr}_{x}\text{I}_{3-x}$  film is proposed in Fig. 1(e), which shows the possible random arrangement of different ligands at the perovskite surface.

A conventional LED device structure of ITO/PEDOT:PSS/ $\text{CsPbBr}_{x}\text{I}_{3-x}$ /PCBM/BCP/Al was adopted for EL studies of the  $\text{CsPbBr}_{x}\text{I}_{3-x}$  films (Fig. 2(a)). The cross-section SEM image of the device architecture in Fig. 2(b) shows small nanoparticles about  $7 \sim 8$  nm in the perovskite layer, which is consistent with the conclusion of XRD and SEM results in Fig. 1(c), S2(a) and S3. Such nano-sized  $\text{CsPbBr}_{x}\text{I}_{3-x}$  crystallites are supposed to preserve the quantum confinement effect, as reported in other  $\text{CsPbBr}_{x}\text{I}_{3-x}$  QD ( $x = 0, 3$ ) systems [11, 32]. In Fig. 2(c), the energy levels of different layers are taken from literature [5, 42, 43]. In the LED structure of this work, the PEDOT:PSS is as the hole injection layer (HIL), the PCBM and a very thin layer of BCP are as the electron injection layers (EIL). We note that in the field of perovskite solar cells, the PEDOT:PSS and PCBM layers showed good carrier extraction properties due to their suitable energy levels with respect to perovskites; and PCBM may also passivate the trap states on perovskite surface and grain boundaries [44–46]. We find that the deposition of the PCBM layer onto the perovskite thin film results in a slightly PL decrease of perovskite thin film, which is proposed to be caused by the carrier extraction effect of PCBM (Fig. S7). In contrast with the carrier extraction process for solar cell applications, charge carriers in LED applications should be injected into the perovskite emitting layer under external applied bias (Fig. S7). The suitable energy levels of PEDOT:PSS and PCBM with  $\text{CsPbBr}_{x}\text{I}_{3-x}$  perovskite facilitate the charge injection process, which is demonstrated by the LED optoelectronic performance as discussed below.

Based on above LED device structure, the as-prepared  $\text{CsPbBr}_{x}\text{I}_{3-x}$  LED shows an EL peak at 659 nm with a FWHM of 40 nm (Fig. 2(d)). The EL spectrum exhibits a slight red-shift relative to the PL spectrum, which is consistent with previous reports of PeLEDs and can be attributed to the interparticle

interaction and Stark effect [6, 24]. The PL quantum yield (PLQY) of the  $\text{CsPbBr}_{x}\text{I}_{3-x}$  thin film is about 15.3%. The CIE coordinates of  $\text{CsPbBr}_{x}\text{I}_{3-x}$  LED are located at CIE (0.711, 0.289) (Fig. 2(e)), which meet the requirement of Rec. 2020 color gamut at CIE (0.708, 0.292) very well [25]. For the  $\text{CsPbBr}_{x}\text{I}_{3-x}$  LED, the current density versus voltage curve in Fig. 2(f) reveals weak current leakage, and the luminance versus voltage curve shows a very low turn-on voltage at 1.6 V. Notably, the turn-on voltage of the  $\text{CsPbBr}_{x}\text{I}_{3-x}$  LED has been greatly reduced from  $>2.7$  V to 1.6 V, in comparison with other reports featuring a conventional LED device structure (Table S1). The turn-on voltage of 1.6 V is lower than the emission photon energy of  $\sim 1.88$ , thereby indicating efficient and barrier-free charge injection into the perovskite emitters [47]. A number of literature of LED devices with different active materials such as perovskites [47, 48] and QDs [49, 50] has reported this sub-bandgap turn-on phenomenon, which is hypothesized to be caused by the Auger-assisted charge injection. Moreover, the  $\text{CsPbBr}_{x}\text{I}_{3-x}$  LED shows a maximum luminance of  $2859 \text{ cd m}^{-2}$  and a maximum EQE value of 8.94%, which have been one of the best cases for the pure-red  $\text{CsPbBr}_{x}\text{I}_{3-x}$  LEDs at CIE (0.711, 0.289) (Table S1) [5, 6]. In addition, an average luminance<sub>max</sub> of  $2708 \text{ cd m}^{-2}$ , and an average EQE<sub>max</sub> of 7.99% are achieved for the  $\text{CsPbBr}_{x}\text{I}_{3-x}$  LEDs as shown in Fig. S8, which demonstrate good reproducibility for the devices.

The EL peaks could be tuned by controlling the annealing temperature of the  $\text{CsPbBr}_{x}\text{I}_{3-x}$  films. For example, annealing the perovskite films at  $85^\circ\text{C}$  or  $110^\circ\text{C}$  would result in  $\text{CsPbBr}_{x}\text{I}_{3-x}$  LEDs (labelled as  $85^\circ\text{C}/110^\circ\text{C}$ - $\text{CsPbBr}_{x}\text{I}_{3-x}$  LEDs) emitting at 650 nm or 673 nm, respectively (Fig. 3(a) and Table 1). The similar phenomenon of emission wavelength difference dependent on film annealing temperature had been also observed in other quasi-2D perovskites and perovskite QD or NC system [38, 51], which is explained by quantum confinement relative to the particle size of nanograins (Fig. S9). Due to quantum confinement, red-shifted emission corresponds to larger crystallite grains, which indicates that higher film annealing temperature results in larger crystallite

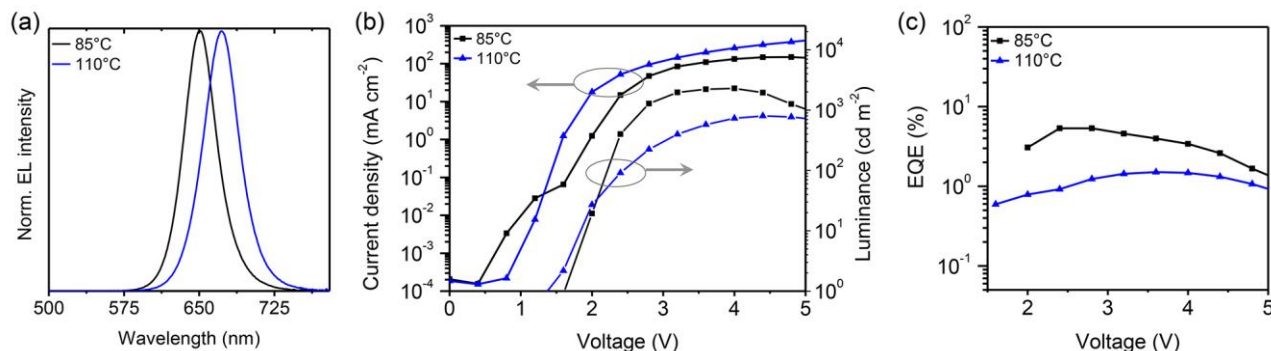


**Figure 3** (a) Normalized EL spectra for the CsPbBr<sub>x</sub>I<sub>3-x</sub> LEDs with different film annealing temperatures at 85°C or 110°C respectively (labeled as 85°C/110°C-CsPbBr<sub>x</sub>I<sub>3-x</sub> LEDs). (b) Current density and luminance versus voltage curves of the 85°C/110°C-CsPbBr<sub>x</sub>I<sub>3-x</sub> LEDs. (c) EQE versus voltage curves of the 85°C/110°C-CsPbBr<sub>x</sub>I<sub>3-x</sub> LEDs.

**Table 1** Summary of the performance of CsPbBr<sub>x</sub>I<sub>3-x</sub> films and LEDs.

Film Annealing Temperature	PLQY (%)	EL peak (nm)	EL FWHM (nm)	Voltage <sub>turn-on</sub> (V)	Luminance <sub>max</sub> (cd m <sup>-2</sup> )	EQE <sub>max</sub> (%)	CIE (x, y)
85°C	15.9	650	38	1.7	2294	5.34	(0.709, 0.290)
100°C	15.3	659	40	1.6	2859	8.94	(0.711, 0.289)
110°C	7.9	673	41	1.6	802	1.51	(0.715, 0.279)

grains in the CsPbBr<sub>x</sub>I<sub>3-x</sub> films. The conclusion is also consistent with the XRD and UV-vis results in Fig. S9. This result is similar as the colloidal CsPbBr<sub>x</sub>I<sub>3-x</sub> ( $x = 0$ ) QD system synthesized in solution, in which higher synthesis temperature results in larger QDs (from 3.4 nm to 12.5 nm), as reported by Luther et al. [11] On the other hand, the shift of emission peak indicates that quantum confinement is preserved in our CsPbBr<sub>x</sub>I<sub>3-x</sub> thin films, which is consistent with previous reports about perovskite thin films featuring nano-sized crystallites with quantum confinement [11, 33, 34]. The 85°C-CsPbBr<sub>x</sub>I<sub>3-x</sub> thin film featuring smaller particle size shows a shorter average PL lifetime of 2.3 ns in comparison with 110°C-CsPbBr<sub>x</sub>I<sub>3-x</sub> thin film showing an average PL lifetime of 6.2 ns (Fig. S9(d)). The PLQY values of the 85°C/110°C-CsPbBr<sub>x</sub>I<sub>3-x</sub> thin films are about 15.9% and 7.9%, respectively. The CIE coordinates of 85°C/110°C-CsPbBr<sub>x</sub>I<sub>3-x</sub> LEDs are (0.709, 0.290) and (0.715, 0.279), respectively (Table 1). In Fig. 3(b), the 110°C-CsPbBr<sub>x</sub>I<sub>3-x</sub> LED shows a low turn-on voltage of 1.6 V. By contrast, the 85°C-CsPbBr<sub>x</sub>I<sub>3-x</sub> LED shows a slightly increased turn-on voltage at about 1.7 V, which is attributed to the slightly bandgap broadening of the CsPbBr<sub>x</sub>I<sub>3-x</sub> film. For 85°C/110°C-CsPbBr<sub>x</sub>I<sub>3-x</sub> LEDs, the maximum luminance values are 2294 cd m<sup>-2</sup> and 802 cd m<sup>-2</sup>, respectively. Correspondingly, the EQE values of 85°C/110°C-CsPbBr<sub>x</sub>I<sub>3-x</sub> LEDs are 5.34% and 1.51%, respectively (Fig. 3(c)). The performance of CsPbBr<sub>x</sub>I<sub>3-x</sub> LEDs is summarized in Table 1. As observed in Table 1, the well-performed CsPbBr<sub>x</sub>I<sub>3-x</sub> LEDs are achieved with the film annealing temperature of 100°C.

EL emission under bias was further studied for the best-performed 100°C-CsPbBr<sub>x</sub>I<sub>3-x</sub> LED. The EL spectra were measured under different voltages firstly. In Fig. 4(a), the EL intensities are enhanced gradually as the voltages are increased to 4.4 V, then reduced. No spectral shift is observed for the CsPbBr<sub>x</sub>I<sub>3-x</sub> LED under operating voltages from 2 V to 7.2 V (Fig. 4(a)). In addition, we further tested the spectral stability of our

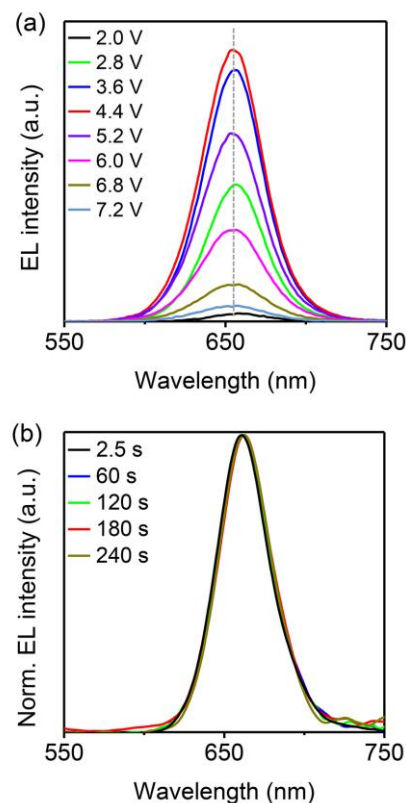


**Figure 4** EL stability of the CsPbBr<sub>x</sub>I<sub>3-x</sub> LED. (a) EL spectra of the CsPbBr<sub>x</sub>I<sub>3-x</sub> LED under different voltages. (b) Normalized EL spectra of the CsPbBr<sub>x</sub>I<sub>3-x</sub> LED at different time under a constant driving voltage of 2.1 V.

LED under a continuous bias voltage of 2.1 V (Fig. S10). As shown in Fig. 4(b), there is no spectral shift for the CsPbBr<sub>x</sub>I<sub>3-x</sub> LED within the test. This result shows a great improvement for the color stability of pure-red CsPbBr<sub>x</sub>I<sub>3-x</sub> based PeLEDs in comparison with previous studies, in which the robust spectral shift of mix-halide CsPbBr<sub>x</sub>I<sub>3-x</sub> LEDs occurred within few

seconds or minutes [5, 6, 27]. For example, Halpert et al. studied the field-driven spectral shift phenomenon of mix-halide  $\text{CsPbBr}_{x-1}\text{I}_{3-x}$  LEDs under a constant operation voltage; in their report, under a high voltage, it took only few seconds to accomplish the red shift from 607 nm to 678 nm [27]. Yao et al. studied the pristine  $\text{CsPbBr}_{x-1}\text{I}_{3-x}$  NC based LEDs, which showed a red-shift of 23 nm swiftly from 638 nm to 661 nm within 3 min under a constant operation voltage [6]. Thus, our  $\text{CsPbBr}_{x-1}\text{I}_{3-x}$  LED shows great potential in sustaining the color purity of pure-red all-inorganic  $\text{CsPbBr}_{x-1}\text{I}_{3-x}$  PeLED. Note that, the operation voltage of the  $\text{CsPbBr}_{x-1}\text{I}_{3-x}$  LEDs in current system is rather low, which benefits from their low turn-on voltage (Table S1). On the other hand, the operational half-lifetime of our LED is about 2.2 min with a relatively high initial luminance of  $\sim 150 \text{ cd m}^{-2}$  at 2.1 V (Fig. S10), which is close to those of pristine  $\text{CsPbBr}_{x-1}\text{I}_{3-x}$  QD based LEDs considering the difference of initial luminance in references [5, 6, 21]. The operational instability is still a challenge. Further exploration combining our advantages in the current system and recent impressive reports to increase the operational lifetime of  $\text{CsPbBr}_{x-1}\text{I}_{3-x}$  LEDs are motivation for future work [6, 21, 52].

### 3 Conclusions

In summary, we firstly developed a  $\text{CsPbBr}_{x-1}\text{I}_{3-x}$  thin film system comprised of nano-sized  $\text{CsPbBr}_{x-1}\text{I}_{3-x}$  crystallites by a typical one-step spin-coating method, which simplified the procedure of preparing  $\text{CsPbBr}_{x-1}\text{I}_{3-x}$  NC based thin films in comparison with the classical colloidal method. The  $\text{CsPbBr}_{x-1}\text{I}_{3-x}$  nanograins were enabled by the surface termination effect of multiple bulky ammonium ligands. Furthermore, we adopted a conventional LED device structure of ITO/PEDOT:PSS/ $\text{CsPbBr}_{x-1}\text{I}_{3-x}$ /PCBM/BCP/Al to fabricate  $\text{CsPbBr}_{x-1}\text{I}_{3-x}$  LED devices. The  $\text{CsPbBr}_{x-1}\text{I}_{3-x}$  thin film based LED exhibited a pure-red color with the CIE coordinates of (0.711, 0.289) at 659 nm, low turn-on voltage of 1.6 V, maximum luminance of  $2859 \text{ cd m}^{-2}$ , and maximum EQE of 8.94%. In addition, the  $\text{CsPbBr}_{x-1}\text{I}_{3-x}$  LED showed improved color stability under operating voltages. Our strategy via the spin-coating method to prepare  $\text{CsPbBr}_{x-1}\text{I}_{3-x}$  thin films incorporated with multiple ammonium ligands paves the way to fabricate color-pure and color-stable all-inorganic PeLEDs.

## 4 Experimental

### 4.1 Chemicals

Cesium iodide (CsI, 99.999%), phenethylammonium iodide (PEAI, 98%), propane-1,3-diammonium bromide (PDAB, 98%), bathocuproine (BCP, 99%) were purchased from Sigma-Aldrich. [6,6]-Phenyl C61 butyric acid methyl ester (PCBM, 99%) was purchased from American Dye Source. Lead iodide ( $\text{PbI}_2$ , 98%), isobutylammonium bromide (IBAB, 98%), N,N-dimethyl-1,3-propanediamine dihydrobromide (DMPDAB, 98%) was purchased from Tokyo Chemical Industry. Dimethyl sulfoxide (DMSO, super dehydrated) was purchased from Wako. Poly(3,4-ethylenedioxythiophene):poly(styrenesulfonate) (PEDOT:PSS, Clevis PVP AI 4083) was purchased from Heraeus. All chemicals were used as received.

### 4.2 Perovskite film and LED fabrication

The patterned-ITO substrates were sequentially sonicated with detergent, deionized water, acetone, and isopropyl alcohol for 20 min, respectively. After drying under a nitrogen flow, the ITO substrates were treated under oxygen plasma for 10 min. A PEDOT:PSS layer was spin-coated onto the ITO substrate at 3500 rpm for 30 s and then baked at  $150^\circ\text{C}$  for 10 min. The ITO/PEDOT:PSS substrates were transferred into a  $\text{N}_2$  glove box. For depositing the perovskite emitting layer, the  $\text{CsPbBr}_{x-1}\text{I}_{3-x}$  precursors incorporating with multiple ammonium ligands were firstly prepared by dissolving 1 mmol of  $\text{PbI}_2$ , 1 mmol of CsI, 0.25 mmol of PEA, 0.25 mmol of IBAB, 0.1 mmol of PDAB and 0.1 mmol of DMPDAB in 3.33 ml of DMSO. Herein, a small amount of Br anion in  $\text{CsPbBr}_{x-1}\text{I}_{3-x}$  was introduced from the organic ammonium bromide in the ligands. The precursor solution was spin-coated onto the ITO/PEDOT:PSS substrates in the glove box at 4500 rpm for 40 s, which were then baked at  $100^\circ\text{C}$  (or  $85^\circ\text{C}/110^\circ\text{C}$  as pointed out in the main text) for 10 min. The as-prepared ITO/PEDOT:PSS/ $\text{CsPbBr}_{x-1}\text{I}_{3-x}$  films were transferred into a vacuum chamber for further thermal evaporation of 40 nm of PCBM and 3 nm of BCP layers sequentially. At last, with a shadow mask, a 100 nm of Al layer was evaporated under a pressure of  $2 \times 10^{-4} \text{ Pa}$ . The active device area was  $0.04 \text{ cm}^2$  as defined by the overlapping area of the ITO and Al electrodes.

### 4.3 Characterization

XRD data were acquired with a Bruker D8 Discover diffractometer using  $\text{Cu K}\alpha$  radiation ( $\lambda = 1.54178 \text{ \AA}$ ). SEM images were acquired using a FEI Helios NanoLab G3 equipment. AFM images were acquired using an ASYLUM-MFP-3D equipment. PL spectra were acquired using a JASCO FP-8500 spectrometer. PL lifetime was measured using the time-correlated, single-photon counting technique (Hamamatsu, C10627), and excitation was provided by a femtosecond mode-locked Ti:sapphire laser (Spectra Physics, MAITAI XFIMW) at 400 nm. PLQY values were acquired using a calibrated integrating sphere system coupled with a JASCO FP-8500 spectrometer. UV-vis spectra were measured using a JASCO V-670 spectrometer. The LED characterization was acquired with a Konica Minolta CS-2000 spectroradiometer coupling with a Keithley source meter (Keithley 2400), which were controlled via a computer (Fig. S11). Thereinto, a Keithley 2400 was used to obtain current density versus voltage data, and the corresponding EL spectra and luminance data were acquired using a Konica Minolta CS-2000 spectroradiometer. The LEDs were tested in air without encapsulation.

## Acknowledgements

This work was supported by funding from the Energy Materials and Surface Sciences Unit of the Okinawa Institute of Science and Technology Graduate University, the OIST Proof of Concept (POC) Program, the OIST R&D Cluster Research Program, and JSPS KAKENHI Grant Number JP18K05266. We would like to thank Dr. Noriko Ishizu, Dr. Takuya Miyazawa and other members in OIST Mechanical Engineering & Micro/Nanofabrication Section for support of device characterization.

**Electronic Supplementary Material:** Supplementary material (LED performance comparison, AFM, UV-vis, SEM, XRD, EL, and



additional LED characterization) is available in the online version of this article at <http://dx.doi.org/xxxxxx>.

## References

- [1] Cao, Y., Wang, N. N., Tian, H., Guo, J. S., Wei, Y. Q., Chen, H., Miao, Y. F., Zou, W., Pan, K., He, Y. R., et al. Perovskite light-emitting diodes based on spontaneously formed submicrometre-scale structures. *Nature* **2018**, *562*, 249-253.
- [2] Lin, K., Xing, J., Quan, L. N., De Arquer, F. P. G., Gong, X., Lu, J., Xie, L., Zhao, W., Zhang, D., Yan, C., et al. Perovskite light-emitting diodes with external quantum efficiency exceeding 20 per cent. *Nature* **2018**, *562*, 245-248.
- [3] Liu, Y., Cui, J., Du, K., Tian, H., He, Z., Zhou, Q., Yang, Z., Deng, Y., Chen, D., Zuo, X., et al. Efficient blue light-emitting diodes based on quantum-confined bromide perovskite nanostructures. *Nat. Photonics* **2019**, *13*, 760-764.
- [4] Zhao, X., Tan, Z.-K. Large-area near-infrared perovskite light-emitting diodes. *Nat. Photonics* **2019**, *14*, 215-218.
- [5] Chiba, T., Hayashi, Y., Ebe, H., Hoshi, K., Sato, J., Sato, S., Pu, Y.-J., Ohisa, S., Kido, J. Anion-exchange red perovskite quantum dots with ammonium iodine salts for highly efficient light-emitting devices. *Nat. Photonics* **2018**, *12*, 681-687.
- [6] Yang, J.-N., Song, Y., Yao, J.-S., Wang, K.-H., Wang, J.-J., Zhu, B.-S., Yang, M.-M., Rahman, S. U., Lan, Y.-F., Fan, F.-J., et al. Potassium-bromide surface passivation on CsPbI<sub>3</sub>Br<sub>2</sub> nanocrystals for efficient and stable pure red perovskite light emitting diodes. *J. Am. Chem. Soc.* **2020**, *142*, 2956-2967.
- [7] Ke, Y., Wang, N., Kong, D., Cao, Y., He, Y., Zhu, L., Wang, Y., Xue, C., Peng, Q., Gao, F., et al. Defect passivation for red perovskite light-emitting diodes with improved brightness and stability. *J. Phys. Chem. Lett.* **2019**, *10*, 380-385.
- [8] Steele, J. A., Jin, H., Dovgaliuk, I., Berger, R. F., Braeckvelt, T., Yuan, H., Martin, C., Solano, E., Lejaeghere, K., Rogge, S. M. J., et al. Thermal unequilibrium of strained black CsPbI<sub>3</sub> thin films. *Science* **2019**, *365*, 679-684.
- [9] Miao, Y., Ke, Y., Wang, N., Zou, W., Xu, M., Cao, Y., Sun, Y., Yang, R., Wang, Y., Tong, Y., et al. Stable and bright formamidinium-based perovskite light-emitting diodes with high energy conversion efficiency. *Nat. Commun.* **2019**, *10*, 3624.
- [10] Wang, Y., Dar, M. I., Ono, L. K., Zhang, T., Kan, M., Li, Y., Zhang, L., Wang, X., Yang, Y., Gao, X., et al. Thermodynamically stabilized  $\beta$ -CsPbI<sub>3</sub>-based perovskite solar cells with efficiencies >18%. *Science* **2019**, *365*, 591-595.
- [11] Swarnkar, A., Marshall, A. R., Sanehira, E. M., Chernomordik, B. D., Moore, D. T., Christians, J. A., Chakrabarti, T., Luther, J. M. Quantum dot-induced phase stabilization of  $\alpha$ -CsPbI<sub>3</sub> perovskite for high-efficiency photovoltaics. *Science* **2016**, *354*, 92-95.
- [12] Wang, Y., Zhang, T., Xu, F., Li, Y., Zhao, Y. A facile low temperature fabrication of high performance CsPbI<sub>2</sub>Br all-inorganic perovskite solar cells. *Solar RRL* **2018**, *2*, 1700180.
- [13] Ma, Q. S., Huang, S. J., Wen, X. M., Green, M. A., Ho-Baillie, A. W. Y. Hole transport layer free inorganic CsPbI<sub>2</sub>Br<sub>2</sub> perovskite solar cell by dual source thermal evaporation. *Adv. Energy Mater.* **2016**, *6*, 1502202.
- [14] Protesescu, L., Yakunin, S., Bodnarchuk, M. I., Krieg, F., Sadhanala, R., Hendon, C. H., Yang, R. X., Walsh, A., Kovalenko, M. V. Nanocrystals of cesium lead halide perovskites (CsPbX<sub>3</sub>, X = Cl, Br, and I): Novel optoelectronic materials showing bright emission with wide color gamut. *Nano Lett.* **2015**, *15*, 3692-3696.
- [15] Li, G. P., Huang, J. S., Li, Y. Q., Tang, J. X., Jiang, Y. Highly bright and low turn-on voltage CsPbBr<sub>3</sub> quantum dot LEDs via conjugation molecular ligand exchange. *Nano Res.* **2019**, *12*, 109-114.
- [16] Li, J. H., Xu, L. M., Wang, T., Song, J. Z., Chen, J. W., Xue, J., Dong, Y. H., Cai, B., Shan, Q. S., Han, B. N., et al. 50-fold EQE improvement up to 6.27% of solution-processed all-inorganic perovskite CsPbBr<sub>3</sub> QLEDs via surface ligand density control. *Adv. Mater.* **2017**, *29*, 1603885.
- [17] Kim, Y. H., Wolf, C., Kim, Y. T., Cho, H., Kwon, W., Do, S., Sadhanala, A., Park, C. G., Rhee, S. W., Im, S. H., et al. Highly efficient light-emitting diodes of colloidal metal-halide perovskite nanocrystals beyond quantum size. *ACS Nano* **2017**, *11*, 6586-6593.
- [18] Zheng, W., Li, Z., Zhang, C., Wang, B., Zhang, Q., Wan, Q., Kong, L., Li, L. Stabilizing perovskite nanocrystals by controlling protective surface ligands density. *Nano Res.* **2019**, *12*, 1461-1465.
- [19] Han, B. N., Cai, B., Shan, Q. S., Song, J. Z., Li, J. H., Zhang, F. J., Chen, J. W., Fang, T., Ji, Q. M., Xu, X. B., et al. Stable, efficient red perovskite light-emitting diodes by ( $\alpha$ ,  $\delta$ )-CsPbI<sub>3</sub> phase engineering. *Adv. Funct. Mater.* **2018**, *28*, 1804285.
- [20] Shen, X., Zhang, Y., Kershaw, S. V., Li, T., Wang, C., Zhang, X., Wang, W., Li, D., Wang, Y., Lu, M., et al. Zn-alloyed CsPbI<sub>3</sub> nanocrystals for highly efficient perovskite light-emitting devices. *Nano Lett.* **2019**, *19*, 1552-1559.
- [21] Yao, J.-S., Ge, J., Wang, K.-H., Zhang, G., Zhu, B.-S., Chen, C., Zhang, Q., Luo, Y., Yu, S.-H., Yao, H.-B. Few-nanometer-sized  $\alpha$ -CsPbI<sub>3</sub> quantum dots enabled by strontium substitution and iodide passivation for efficient red-light emitting diodes. *J. Am. Chem. Soc.* **2019**, *141*, 2069-2079.
- [22] Lu, M., Zhang, X., Zhang, Y., Guo, J., Shen, X., Yu, W. W., Rogach, A. L. Simultaneous strontium doping and chlorine surface passivation improve luminescence intensity and stability of CsPbI<sub>3</sub> nanocrystals enabling efficient light-emitting devices. *Adv. Mater.* **2018**, *30*, 1804691.
- [23] Zhang, X. Y., Sun, C., Zhang, Y., Wu, H., Ji, C. Y., Chuai, Y. H., Wang, P., Wen, S. P., Zhang, C. F., Yu, W. W. Bright perovskite nanocrystal films for efficient light-emitting devices. *J. Phys. Chem. Lett.* **2016**, *7*, 4602-4610.
- [24] Pan, J., Shang, Y. Q., Yin, J., De Bastiani, M., Peng, W., Dursun, I., Sinatra, L., El-Zohry, A. M., Hedhili, M. N., Emwas, A. H., et al. Bidentate ligand-passivated CsPbI<sub>3</sub> perovskite nanocrystals for stable near-unity photoluminescence quantum yield and efficient red light-emitting diodes. *J. Am. Chem. Soc.* **2018**, *140*, 562-565.
- [25] Zhu, R., Luo, Z., Chen, H., Dong, Y., Wu, S.-T. Realizing rec. 2020 color gamut with quantum dot displays. *Opt. Express* **2015**, *23*, 23680-23693.
- [26] Chang, J., Zhang, S. T., Wang, N. N., Sun, Y., Wei, Y. Q., Li, R. Z., Yi, C., Wang, J. P., Huang, W. Enhanced performance of red perovskite light-emitting diodes through the dimensional tailoring of perovskite multiple quantum wells. *J. Phys. Chem. Lett.* **2018**, *9*, 881-886.
- [27] Vashishtha, P., Halpert, J. E. Field-driven ion migration and color instability in red-emitting mixed halide perovskite nanocrystal light-emitting diodes. *Chem. Mater.* **2017**, *29*, 5965-5973.
- [28] Samu, G. F., Balog, Á., De Angelis, F., Meggiolaro, D., Kamat, P. V., Janáky, C. Electrochemical hole injection selectively expels iodide from mixed halide perovskite films. *J. Am. Chem. Soc.* **2019**, *141*, 10812-10820.
- [29] Knight, A. J., Wright, A. D., Patel, J. B., McMeekin, D. P., Snaith, H. J., Johnston, M. B., Herz, L. M. Electronic traps and phase segregation in lead mixed-halide perovskite. *ACS Energy Lett.* **2019**, *4*, 75-84.
- [30] He, Z., Liu, Y., Yang, Z., Li, J., Cui, J., Chen, D., Fang, Z., He, H., Ye, Z., Zhu, H., et al. High-efficiency red light-emitting diodes based on multiple quantum wells of phenylbutylammonium-cesium lead iodide perovskites. *ACS Photonics* **2019**, *6*, 587-594.
- [31] Xing, J., Zhao, Y., Askerka, M., Quan, L. N., Gong, X., Zhao, W., Zhao, J., Tan, H., Long, G., Gao, L., et al. Color-stable highly luminescent sky-blue perovskite light-emitting diodes. *Nat. Commun.* **2018**, *9*, 3541.
- [32] Jiang, M. W., Hu, Z. H., Liu, Z. H., Wu, Z. F., Ono, L. K., Qi, Y. B. Engineering green-to-blue emitting CsPbBr<sub>3</sub> quantum-dot films with efficient ligand passivation. *ACS Energy Lett.* **2019**, *4*, 2731-2738.
- [33] Xiao, Z. G., Kerner, R. A., Tran, N., Zhao, L. F., Scholes, G. D., Rand, B. P. Engineering perovskite nanocrystal surface termination for light-emitting diodes with external quantum efficiency exceeding 15%. *Adv. Funct. Mater.* **2019**, *29*, 1807284.
- [34] Xiao, Z. G., Kerner, R. A., Zhao, L. F., Tran, N. L., Lee, K. M., Koh, T. W., Scholes, G. D., Rand, B. P. Efficient perovskite light-emitting diodes featuring nanometre-sized crystallites. *Nat. Photonics* **2017**, *11*, 108-115.
- [35] Li, F. M., Pei, Y. H., Xiao, F., Zeng, T. X., Yang, Z., Xu, J. J., Sun, J., Peng, B., Liu, M. Z. Tailored dimensionality to regulate the phase stability of inorganic cesium lead iodide perovskites. *Nanoscale* **2018**, *10*, 6318-6322.
- [36] Si, J., Liu, Y., He, Z., Du, H., Du, K., Chen, D., Li, J., Xu, M., Tian, H., He, H., et al. Efficient and high-color-purity light-emitting diodes based on in situ grown films of CsPbX<sub>3</sub> (X = Br, I) nanoplates with controlled thicknesses. *ACS Nano* **2017**, *11*, 11100-11107.
- [37] Xiao, Z. G., Zhao, L. F., Tran, N. L., Lin, Y. H. L. S., Silver, S. H., Kerner, R. A., Yao, N., Kahn, A., Scholes, G. D., Rand, B. P. Mixed-halide perovskites with stabilized bandgaps. *Nano Lett.* **2017**, *17*, 6863-6869.



- [38] Lin, H., Mao, J., Qin, M., Song, Z., Yin, W., Lu, X., Choy, W. C. H. Single-phase alkylammonium cesium lead iodide quasi-2D perovskites for color-tunable and spectrum-stable red LEDs. *Nanoscale* **2019**, *11*, 16907-16918.
- [39] Shang, Y. Q., Li, G., Liu, W. M., Ning, Z. J. Quasi-2D inorganic CsPbBr<sub>3</sub> perovskite for efficient and stable light-emitting diodes. *Adv. Funct. Mater.* **2018**, *28*, 1801193.
- [40] Tian, Y., Zhou, C., Worku, M., Wang, X., Ling, Y., Gao, H., Zhou, Y., Miao, Y., Guan, J., Ma, B. Highly efficient spectrally stable red perovskite light-emitting diodes. *Adv. Mater.* **2018**, *30*, 1707093.
- [41] Yang, Y., Qin, H., Jiang, M., Lin, L., Fu, T., Dai, X., Zhang, Z., Niu, Y., Cao, H., Jin, Y., et al. Entropic ligands for nanocrystals: From unexpected solution properties to outstanding processability. *Nano Lett.* **2016**, *16*, 2133-2138.
- [42] Malinkiewicz, O., Yella, A., Lee, Y. H., Espallargas, G. M., Graetzel, M., Nazeeruddin, M. K., Bolink, H. J. Perovskite solar cells employing organic charge-transport layers. *Nat. Photonics* **2014**, *8*, 128-132.
- [43] Chen, C. L., Zhang, S. S., Wu, S. H., Zhang, W. J., Zhu, H. M., Xiong, Z. Z., Zhang, Y. J., Chen, W. Effect of BCP buffer layer on eliminating charge accumulation for high performance of inverted perovskite solar cells. *RSC Adv.* **2017**, *7*, 35819-35826.
- [44] Xu, J., Buin, A., Ip, A. H., Li, W., Voznyy, O., Comin, R., Yuan, M., Jeon, S., Ning, Z., McDowell, J. J., et al. Perovskite–fullerene hybrid materials suppress hysteresis in planar diodes. *Nat. Commun.* **2015**, *6*, 7081.
- [45] Shao, Y., Xiao, Z., Bi, C., Yuan, Y., Huang, J. Origin and elimination of photocurrent hysteresis by fullerene passivation in CH<sub>3</sub>NH<sub>3</sub>PbI<sub>3</sub> planar heterojunction solar cells. *Nat. Commun.* **2014**, *5*, 5784.
- [46] Wang, Q., Shao, Y., Dong, Q., Xiao, Z., Yuan, Y., Huang, J. Large fill-factor bilayer iodine perovskite solar cells fabricated by a low-temperature solution-process. *Energy Environ. Sci.* **2014**, *7*, 2359-2365.
- [47] Wang, J., Wang, N., Jin, Y., Si, J., Tan, Z.-K., Du, H., Cheng, L., Dai, X., Bai, S., He, H., et al. Interfacial control toward efficient and low-voltage perovskite light-emitting diodes. *Adv. Mater.* **2015**, *27*, 2311-2316.
- [48] Li, J., Shan, X., Bade, S. G. R., Geske, T., Jiang, Q., Yang, X., Yu, Z. Single-layer halide perovskite light-emitting diodes with sub-band gap turn-on voltage and high brightness. *J. Phys. Chem. Lett.* **2016**, *7*, 4059-4066.
- [49] Mashford, B. S., Stevenson, M., Popovic, Z., Hamilton, C., Zhou, Z., Breen, C., Steckel, J., Bulovic, V., Bawendi, M., Coe-Sullivan, S., et al. High-efficiency quantum-dot light-emitting devices with enhanced charge injection. *Nat. Photonics* **2013**, *7*, 407-412.
- [50] Pradhan, S., Dalmases, M., Konstantatos, G. Origin of the below-bandgap turn-on voltage in light-emitting diodes and the high VOC in solar cells comprising colloidal quantum dots with an engineered density of states. *J. Phys. Chem. Lett.* **2019**, *10*, 3029-3034.
- [51] Scheidt, R. A., Atwell, C., Kamat, P. V. Tracking transformative transitions: From CsPbBr<sub>3</sub> nanocrystals to bulk perovskite films. *ACS Mater. Lett.* **2019**, *1*, 8-13.
- [52] Zou, Y., Yuan, Z., Bai, S., Gao, F., Sun, B. Recent progress toward perovskite light-emitting diodes with enhanced spectral and operational stability. *Mater. Today Nano* **2019**, *5*, 100028.